The non-local nature of structure functions

P.-Å. Krogstad[1] and P.A. Davidson[2]

[1]Dept. Energy and Process Engineering, Norwegian University of Science and Technology
N-7491 Trondheim, Norway
[2]Dept. Engineering, University of Cambridge
Cambridge CB2 1PZ, U.K.

Abstract

Kolmogorov's two-thirds, $\langle (\Delta v)^2 \rangle \sim \varepsilon^{2/3} r^{2/3}$, and five-thirds, $E \sim \varepsilon^{2/3} k^{-5/3}$, laws are formally equivalent in the limit of vanishing viscosity, $\nu \to 0$. However, for most Reynolds numbers encountered in laboratory scale experiments, or numerical simulations, it is invariably easier to observe the five-thirds law. By creating artificial fields of isotropic turbulence composed of a random sea of Gaussian eddies whose size and energy distribution can be controlled, we show why this is the case. The energy of eddies of scale, s, is shown to vary as $s^{2/3}$, in accordance with Kolmogorov's 1941 law, and we vary the range of scales, $\gamma = s_{max}/s_{min}$, in any one realisation from $\gamma = 25$ to $\gamma = 800$. This is equivalent to varying the Reynolds number in an experiment from $R_\lambda = 60$ to $R_\lambda = 600$. While there is some evidence of a five-thirds law for $\gamma > 50$ ($R_\lambda > 100$), the two-thirds law only starts to become apparent when γ approaches 200 ($R_\lambda \sim 240$). The reason for this discrepancy is that the second-order structure function is a poor filter, mixing information about energy and enstrophy, and from scales larger and smaller than r. In particular, in the inertial range, $\langle (\Delta v)^2 \rangle$ takes the form of a mixed power-law, $a_1 + a_2 r^2 + a_3 r^{2/3}$, where $a_2 r^2$ tracks the variation in enstrophy and $a_3 r^{2/3}$ the variation in energy. These findings are shown to be consistent with experimental data where the polution of the $r^{2/3}$ law by the enstrophy contribution, $a_2 r^2$, is clearly evident. We show that higher-order structure functions (of even order) suffer from a similar deficiency. (See also [2].)

Introduction

There are three diagnostic tools commonly used to give an impression of the variation of energy with eddy size in isotropic turbulence. They are the three-dimensional energy spectrum, $E(k)$, the one-dimensional energy spectrum, $F_{11}(k)$, and the second-order structure function, $\langle (\Delta v)^2 \rangle (r)$. However, it is well-known that all three diagnostic tools give imperfect measures of the scale-by-scale energy distribution. For example, consider an artificial field of turbulence composed of a sea of eddies (i.e. blobs of vorticity) of fixed size ℓ_e. For simplicity we shall take the vortex blobs to have a Gaussian velocity distribution,

$$\mathbf{u} = \Omega r \exp\left[-2r^2/\ell_e^2\right] \hat{\mathbf{e}}_\theta, \tag{1}$$

though the results would be little changed if we had chosen a different profile. (Here $\hat{\mathbf{e}}_\theta$ is the unit vector in the azimuthal direction.) If these eddies are randomly located and orientated then we find (see [1]),

$$E(k) = \frac{\langle \mathbf{u}^2 \rangle \ell_e}{24\sqrt{\pi}} (k\ell_e)^4 \exp\left[-(k\ell_e)^2/4\right]. \tag{2}$$

Evidently, eddies of a given size contribute to all wavenumbers in $E(k)$, their contribution not being restricted to wavenumbers of order $k \sim 1/\ell_e$. Fortunately, however, Eq. (2) is sharply peaked around $k \sim \pi/\ell_e$, and so this is a deficiency of $E(k)$

which is frequently overlooked. However, the shortcomings of $F_{11}(k)$ and $\langle (\Delta v)^2 \rangle$ are not so readily dismissed. It may be shown that (see, for example, [4]),

$$E(k) = k^3 \frac{d}{dk}\left[\frac{1}{k}\frac{dF_{11}}{dk}\right] \tag{3}$$

$$F_{11}(k) = \frac{1}{2}\int_k^\infty \left[1 - (k/k^*)^2\right]\frac{E(k^*)}{k^*}dk^* \tag{4}$$

and so $F_{11}(k)$ represents the weighted sum of $E(k^*)$, integrated from $k^* = k$ to $k^* = \infty$. Thus $F_{11}(k)$ systematically and artificially shifts energy to small k, with $F_{11}(k)$ peaked at $k = 0$. For a random sea of Gaussian eddies of fixed size ℓ_e we find, from Eq. (2) and (3),

$$F_{11}(k) = \frac{\langle \mathbf{u}^2 \rangle \ell_e}{6\sqrt{\pi}} \exp\left[-(k\ell_e)^2/4\right]. \tag{5}$$

Evidently, in real turbulence, $F_{11}(k)$ provides a flawed measure of the distribution of energy across the different eddy sizes.

The situation is no better with $\langle (\Delta v)^2 \rangle$, where (see [1]),

$$\frac{3}{4}\langle (\Delta v)^2 \rangle (r) \approx \int_{\pi/r}^\infty E(k)dk + (r/\pi)^2 \int_0^{\pi/r} k^2 E(k)dk. \tag{6}$$

In words, $\frac{3}{4}\langle (\Delta v)^2 \rangle$ represents the energy held below scale r, plus $(r/\pi)^2$ times the enstrophy held above scale r. Thus $\langle (\Delta v)^2 \rangle$ mixes information about energy and enstrophy, and information about scales smaller and larger than r. So the usual interpretation of $\langle (\Delta v)^2 \rangle$, as the cumulative energy held below scale r ([3],[5]) is, at best, a crude approximation. More generally, we see that $\langle (\Delta v)^2 \rangle (r)$ is a very leaky filter, admitting information from all scales.

In the limit of Re $\to \infty$, the differences between the various diagnostics is often unimportant in the inertial range as a power-law in $E(k)$ gives rise to the same power-law exponent in F_{11}, and a corresponding power-law in $\langle (\Delta v)^2 \rangle$. For example, the five-thirds law, $E = \alpha\varepsilon^{2/3}k^{-5/3}$, corresponds to $F_{11} = \alpha_{11}\varepsilon^{2/3}k^{-5/3}$ and $\langle (\Delta v)^2 \rangle = \beta\varepsilon^{2/3}r^{2/3}$, where $\alpha = 0.761\beta = 55\alpha_{11}/9$. However, at the finite values of Re encountered in numerical simulations and experiments, a power-law in $E(k)$ need not correspond to clear power-laws in $F_{11}(k)$ or $\langle (\Delta v)^2 \rangle$. In this paper we investigate the limitations of $F_{11}(k)$ and $\langle (\Delta v)^2 \rangle$ in detecting inertial-range energy distributions at finite Re.

Our central finding is that, in the inertial range, $\langle (\Delta v)^2 \rangle$ takes the form of a mixed power-law of the form

$$\langle (\Delta v)^2 \rangle = a_1 + a_2 r^2 + a_3 r^{2/3}, \tag{7}$$

where $a_2 r^2$ tracks the scale-by-scale variations in enstrophy while $a_3 r^{2/3}$ follows the variation in energy. The pollution of the $r^{2/3}$ law by $a_2 r^2$ is clearly evident in the experimental data presented.

Deficiencies of the Second-Order Structure Function

An Idealised Model Problem

In this section we examine a somewhat artificial model problem, designed to expose the weaknesses in $F_{11}(k)$ and $\langle (\Delta v)^2 \rangle$ which arise at finite Re. Consider an artificial field of isotropic turbulence composed of a random sea of vortex blobs, which we take to be Gaussian eddies, $\mathbf{u} = \Omega r \exp[-2\mathbf{x}^2/s^2]\, \hat{\mathbf{e}}_\theta$ in (r, θ, z) coordinates. Let the eddies be randomly but uniformly distributed in space, randomly orientated, and have variable energy and size, s. Also, let $\hat{E}(s)$ be the energy density of the turbulence, in the sense that $\hat{E}(s)ds$ gives the average kinetic energy held in the size range $s \to s + ds$, and

$$\frac{1}{2}\langle \mathbf{u}^2 \rangle = \int_0^\infty \hat{E}(s)ds. \tag{8}$$

Then it may be shown that (see [1]),

$$E(k) = \int_0^\infty \frac{\hat{E}(s)s}{12\sqrt{\pi}}(ks)^4 \exp[-(ks)^2/4]ds \tag{9}$$

$$F_{11}(k) = \int_0^\infty \frac{\hat{E}(s)s}{3\sqrt{\pi}} \exp[-(ks)^2/4]ds \tag{10}$$

$$\frac{3}{4}\langle (\Delta v)^2 \rangle = \int_0^\infty \hat{E}(s)[1 - \exp(-r^2/s^2)]ds \tag{11}$$

Now we are interested in the consequences for E, F_{11} and $\langle (\Delta v)^2 \rangle$ of truncating the range of eddy sizes. Suppose, therefore, that the range of eddy sizes is restricted to $\ell < s < L$, with a low L/ℓ corresponding to a small value of Re, and a large L/ℓ to a high value of Re. Moreover, suppose that the kinetic energy held in each decade of scale varies as the power-law s^n, i.e.

$$s\hat{E}(s) = \begin{cases} \kappa s^n; & \ell < s < L \\ 0; & s < \ell, s > L \end{cases} \tag{12}$$

Then Eq. (9)-(11) are readily integrated to give,

$$I_1(k) = E(k)/E^\infty(k) = \frac{1}{\Gamma(a)}\int_{(k\ell/2)^2}^{(kL/2)^2} t^{a-1}e^{-t}dt \tag{13}$$

$$I_2(k) = F_{11}(k)/F_{11}^\infty(k) = \frac{1}{\Gamma(b)}\int_{(k\ell/2)^2}^{(kL/2)^2} t^{b-1}e^{-t}dt \tag{14}$$

$$\frac{(3/4)\langle (\Delta v)^2 \rangle}{\langle \mathbf{u}^2 \rangle/2} = \frac{nr^n}{L^n - \ell^n}\int_{\ell/r}^{L/r} t^{n-1}\left[1 - \exp(-1/t^2)\right]dt \tag{15}$$

where $a = \frac{1}{2}(n+5)$, $b = \frac{1}{2}(n+1)$ and Γ is the gamma function. Here $E^\infty(k)$ and $F_{11}^\infty(k)$ are the functional forms of E and F_{11} in the limit of $L/\ell \to \infty$ with $\ell << k^{-1} << L$:

$$E^\infty(k) = \frac{2^{n+2}\kappa\Gamma(a)}{3\sqrt{\pi}}k^{-(n+1)} \tag{16}$$

$$F_{11}^\infty(k) = \frac{2^n \kappa\Gamma(b)}{3\sqrt{\pi}}k^{-(n+1)} \tag{17}$$

Since E^∞ and F_{11}^∞ are merely power-laws in k, we may regard I_1 and I_2 as so-called compensated forms of E and F_{11}, with $I_1 = I_2 = 1$ for $L/\ell \to \infty$. In the remainder of this section we shall take $n = 2/3$, corresponding to Kolmogorov's 1941 law. In such a case, $E^\infty \sim F_{11}^\infty \sim k^{-5/3}$.

There now arises the issue of how we might relate the size range, $\gamma = L/\ell$, to the Reynolds number in an experiment, such as grid turbulence. Let L be the eddy size at the top of the inertial range, ℓ the eddy size at the bottom of the inertial range,
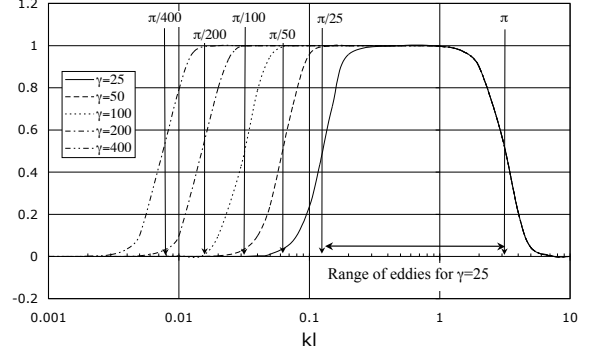

Figure 1: Compensated spectra $I_1 \sim k^{5/3}E(k)$ as a function of $k\ell$.
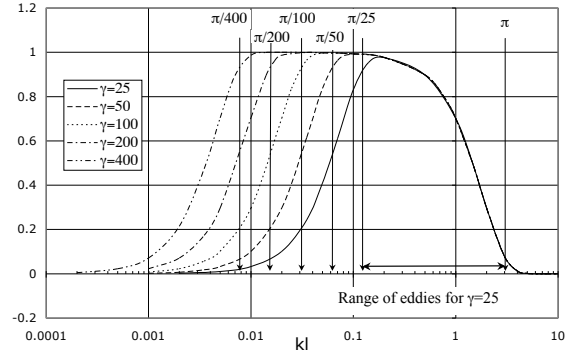

Figure 2: Compensated spectra $I_2 \sim k^{5/3}F_{11}(k)$ as a function of $k\ell$.

and η be the Kolmgorov scale, $(\nu^3/\varepsilon)^{1/4}$. Then we expect $\varepsilon = Au^3/L$ and $\ell = a\eta$ where ε is the rate of dissipation of turbulent kinetic energy. A and a are dimensionless coefficients, $u = \sqrt{<u_x^2>}$, ν is the viscosity, and we have assumed that the integral scale of the turbulence is of order L. We expect the coefficients A and a to be of order unity, with a universal but A non-universal, i.e. different for different grid geometries. In terms of the Taylor microscale, λ, we have $\lambda^2 = \frac{15\nu u^2}{\varepsilon} = \frac{15\nu u^2}{Au^3/L}$. This allows us to express γ in terms of the two Reynolds numbers $Re = uL/\nu$ and $R_\lambda = u\lambda/\nu$. After a little algebra we find

$$\gamma = L/\ell = (A^{1/4}/a)Re^{3/4} = \left(\frac{A}{15^{3/4}a}\right)R_\lambda^{3/2}. \tag{18}$$

We shall see later that grid turbulence experiments suggest that $A/a \approx 0.34 \to 0.45$, depending on the type of grid used. Taking a mean value of $A/a = 0.4$ we have $\gamma \approx 0.0525R_\lambda^{3/2}$.

Figures 1 and 2 show the compensated energy spectra, $I_1 \sim k^{5/3}E(k)$ and $I_2 \sim k^{5/3}F_{11}(k)$, respectively, as a function of $k\ell$ for $\gamma = 25$ to 400. The vertical lines at π/γ and π indicate the range of eddies present in each case. It is evident that, in this model problem, $E(k)$ displays a clear $k^{-5/3}$ law (corresponding to $I_1 = 1$) for $\gamma \geq 50$. The one-dimensional spectrum does less well, systematically and artificially displacing energy to low wavenumbers, as expected. Nevertheless, F_{11} shows evidence of a $k^{-5/3}$ law for $\gamma \geq 200$ (i.e. $R_\lambda \geq 240$).

Figure 3 shows $\langle (\Delta v)^2 \rangle$, normalised by $2u^2$, as a function of r/ℓ for $\gamma = 50, 200, 400$ and 800, the arrows at $r/\ell = 1$ and $r/\ell = \gamma$
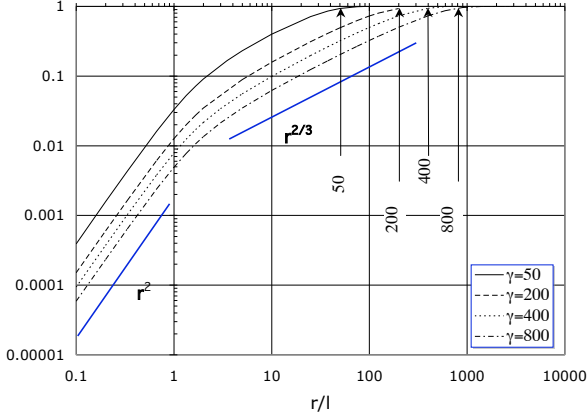
Figure 3: Normalised structure function, $\langle(\Delta v)^2\rangle /2u^2$, as a function of r/ℓ; $\gamma = 50$, 200, 400 and 800.
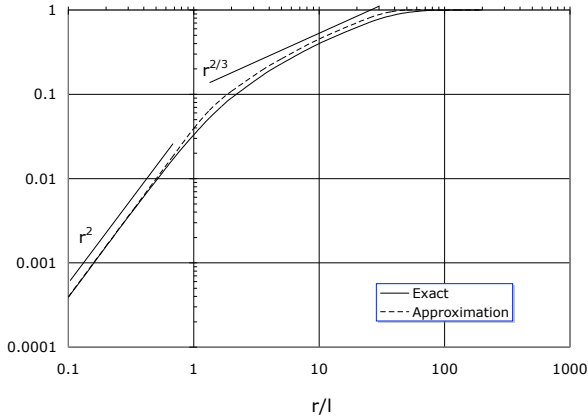

Figure 4: Comparison of $\langle(\Delta v)^2\rangle /2u^2$ with approximation (19)-(21) for $\gamma = 50$.

indicating the range of eddies in each case. There is no clear $r^{2/3}$ law at $\gamma = 50$ and we do not obtain a decade of $r^{2/3}$ until γ reaches ~ 400 ($R_\lambda \approx 390$). Notice also the $\langle(\Delta v)^2\rangle \sim r^2$ region to the left of $r/\ell = 1$. Clearly, in this model problem, $\langle(\Delta v)^2\rangle$ is an inferior diagnostic tool.

The mixing of information about energy and enstrophy

We have already suggested that this failure in $\langle(\Delta v)^2\rangle$ arises from the fact that the second-order structure function mixes information about energy and enstrophy in accordance with Eq. (6). We may confirm this as follows. The energy spectrum does a reasonable job of tracking the energy distribution for $\gamma \geq 50$, so let us approximate $E(k)$ by $E(k) = \kappa k^{-5/3}$, $\pi/L \leq k \leq \pi/\ell$, while $E(k) = 0$ outside this range. Then Eq. (6) yields,

$$\frac{(3/4)\langle(\Delta v)^2\rangle}{<\mathbf{u}^2>/2} \approx \frac{1-\gamma^{-4/3}}{2(\gamma^{2/3}-1)}\left(\frac{r}{\ell}\right)^2 \quad , \quad r < \ell \qquad (19)$$

$$\frac{(3/4)\langle(\Delta v)^2\rangle}{<\mathbf{u}^2>/2} \approx \frac{3(r/\ell)^{2/3}-2-\gamma^{-4/3}(r/\ell)^2}{2(\gamma^{2/3}-1)} \quad , \quad \ell < r < L \qquad (20)$$

$$\frac{(3/4)\langle(\Delta v)^2\rangle}{<\mathbf{u}^2>/2} \approx 1 \quad , \quad r > L \qquad (21)$$

which is compared with the exact distribution of $\langle(\Delta v)^2\rangle$ in Figure 4 for $\gamma = 50$.

Evidently, Eq. (19) - (21) is a good approximation to Eq. (15), and it has the advantage over the exact distribution in that it makes explicit the reason for the failure of $\langle(\Delta v)^2\rangle$. Equation (19) shows that, for $r < \ell$, the structure function has nothing to do with energy, but rather reflects the total enstrophy of the population of eddies. Conversely, for $r > L$, the structure function has nothing to do with enstrophy, but rather measures the total energy. For $\ell < r < L$, Eq. (20), there is a mixture of two power-laws, $r^{2/3}$ and r^2, with the former tracking the energy of the eddies and the latter tracking the enstrophy in accordance with Eq. (6). Thus the failure of $\langle(\Delta v)^2\rangle$ to display a clear $r^{2/3}$ law at modest values of γ arises from the contamination of the structure function by enstrophy, as measured by the second integral on the right of Eq. (6). Note that, as $\gamma \to \infty$ in Eq. (20), we recover the two-thirds law for $r << L$. However, we still get mixed power-law behaviour when r/L is of order unity, even in the limit of $\gamma \to \infty$.

We note in passing that, if we had adopted the conventional interpretation of $\langle(\Delta v)^2\rangle$, as the cumulative energy held below scale r, ([5], [3]), i.e. $\frac{3}{4}\langle(\Delta v)^2\rangle(r) \approx \int_{\pi/r}^{\infty} E(k)dk$, then Eq. (20) simplifies to

$$\frac{(3/4)\langle(\Delta v)^2\rangle}{<\mathbf{u}^2>/2} \approx \frac{(r/\ell)^{2/3}-1}{\gamma^{2/3}-1} \quad , \quad \ell < r < L \qquad (22)$$

and the mixed power-law disappears. We shall compare both Eq. (20) and (22) with experimental data later. While Eq. (20) is an excellent fit to the data, Eq. (22) is not.
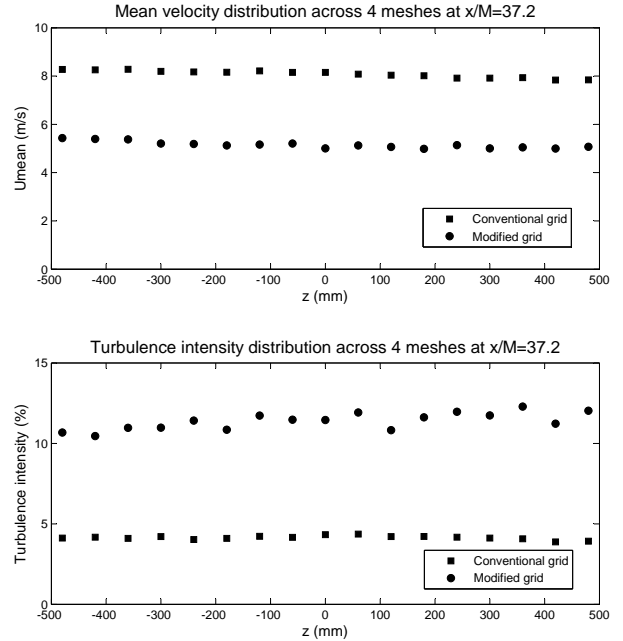

Figure 5: Mean velocity and turbulence intensity distributions across the flow at $x/M = 37.2$. Squares: Conventional grid, Circles: Modified grid.

Comparison With Experimental Data

The model problem described above is much too idealised to be considered representative of real turbulence. Never-the-less, the central notion embedded in Eq. (6), that $\langle(\Delta v)^2\rangle$ mixes information about enstrophy and energy, is robust. We might
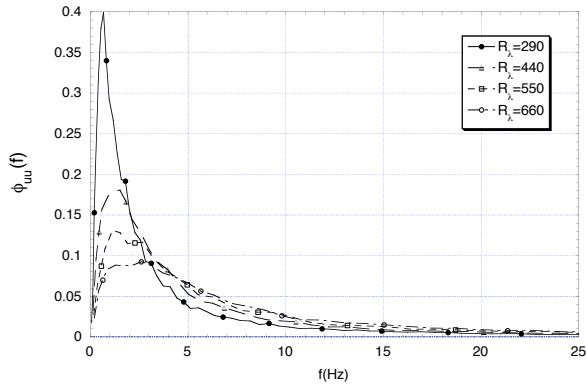
Figure 6: Low frequency part of the power density spectra.

expect, therefore, that real turbulence exhibits a behaviour not unlike Eq. (19) → (21), with a mixed power-law in the inertial range.

In order to test this idea, a set of experiments were performed in grid generated turbulence. The measurements were performed in the large wind tunnel at The Norwegian University of Science and Technology, which has a test section $2m$ high by $2.7m$ wide, with a length of $11m$. Two grids were used. One was a conventional grid made of square bars $46 \times 46mm$ forming a square mesh with a mesh size of $240mm$. In order to make the turbulent Reynolds number as high as possible, a second grid was created from the first by blocking every alternate mesh. This increased the grid solidity from 34.7% to 67.3%. The measurements were performed at $x = 9.3m$ from the grid, corresponding to $x/M = 37.2$. With the conventional grid the tunnel speed was restricted to $U = 18.5m/s$. Due to the significant blocking caused by the second grid, this dropped to about $U = 12m/s$ when the modified grid was installed. Measurements were made for $180 \le R_\lambda \le 320$ using the conventional grid and $290 \le R_\lambda \le 660$ with the modified grid.

The measurements were taken using $2.5\mu m$ single hot wires with a ratio of wire length, w, to Kolmogorov length scale, η, ranging from $w/\eta = 0.9$ to 2.9. From initial measurements of the power density spectra at high sampling rates, the point where electronic noise started to affect the dissipation spectrum was determined. The signal was then low-pass filtered at this frequency and the sampling frequency was set slightly higher than twice the cut-off frequency.

The severe blocking of the second grid may cause a concern about the flow homogenity. To check the uniformity at the measurement station, a number of spanwise traverses were made across 4 meshes for both grids at $x/M = 37.2$. Figure 5 shows that the uniformity of both the mean velocity and the turbulence intensity were about the same for both grids.

It is known that high grid solidity may cause a flapping motion in the flow that is caused by the interaction of the jets formed by the grid. This will show up as isolated peaks of increased energy in the low frequency part of the spectrum. The shedding frequency is expected to depend linearly on the flow velocity and should therefore be found in the power spectra at increasing frequency as the velocity is increased. Figure 6 shows the low frequency part of the spectra for a range of mean velocities from about $U = 2.5$ to 10m/s. Assuming $f_{flapping} \sim U/M$ we would expect the range of frequencies to be roughly from 10 to 40Hz. There are no indications of a velocity dependent energy peak in
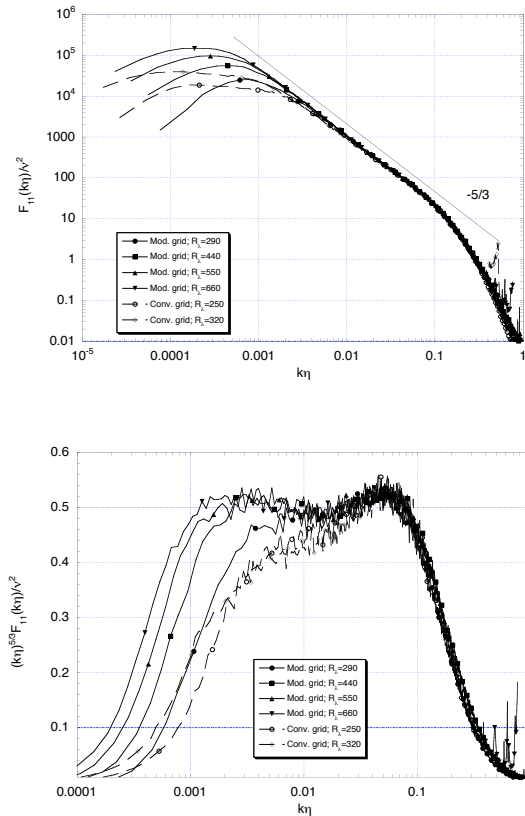

Figure 7: (a) Power density spectra. (b) Compensated power density spectra..

the plotted energy distributions. (The full range power density spectra are shown in Figure 7.)

For each test condition the signal was sampled in 6 batches of about 4×10^6 samples to ensure that the full range of the energy spectrum was resolved. Figure 7 shows a selection of the measured Kolmogorov scaled streamwise one-dimensional spectrum as function of Reynolds number for both grids. The collapse is seen to be quite good and for the highest R_λ the inertial sub range covers about two decades of k. The corresponding second order structure functions are shown in Figure 8.

The dissipation rate, ε, used to estimate the Kolmogorov scales, were obtained using three independent methods. Assuming small scale isotropy, ε was computed from $\varepsilon_1 = \frac{15\nu}{U^2}\langle(\partial u/\partial t)^2\rangle$. The second estimate was obtained by integrating the dissipation spectrum, $\varepsilon_2 = 15\nu \int_0^\infty k_1^2 F_{11}(k_1)dk_1$. Finally, ε was estimated from the inertial subrange using $F_{11}(k_1) = C_1\varepsilon_3^{2/3}k_1^{-5/3}$ with $C_1 = 0.52$. The three estimates agreed for all cases to within +/- 10 %; most of the time even better.

The issue now arises as to whether or not the measured structure functions exhibit a mixed power-law behaviour of the form suggested by Eq. (6) and Eq. (19) → (21). In short, does $\langle(\Delta v)^2\rangle$ take the form

$$\langle(\Delta v)^2\rangle \sim a_1 + a_2r^2 + a_3r^{2/3} \qquad (23)$$

in the inertial subrange? Despite the naivity of the model problem outlined earlier, it seems natural to compare the data directly with predictions Eq. (19) → (21). This has the advantage that Eq. (19) → (21) contain only one free parameter, as we shall now show.
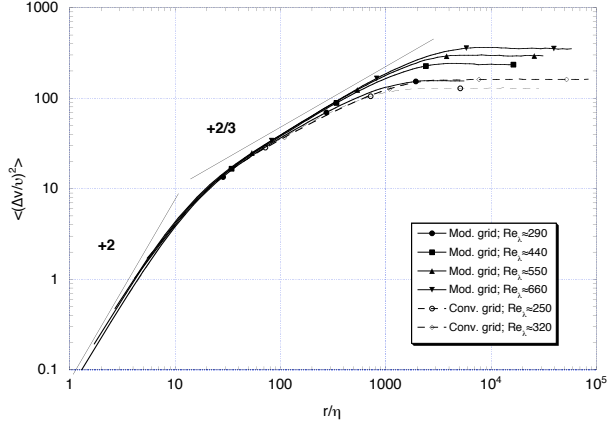
Figure 8: Measured $\langle(\Delta v)^2\rangle$ scaled with Kolmogorov variables.

The right-hand-sides of Eq. (19) $\rightarrow$ (21) contain the unknowns γ and ℓ. However, these are not independent as Eq. (19) must be compatible with

$$\frac{(3/4)\langle(\Delta v)^2\rangle}{\langle \mathbf{u}^2\rangle/2} \rightarrow \frac{r^2}{2\lambda^2} \qquad (24)$$

for $r \rightarrow 0$, and this demands that

$$\ell^2 = \frac{1-\gamma^{-4/3}}{\gamma^{2/3}-1}\lambda^2 \; . \qquad (25)$$

Moreover we have seen that

$$\gamma = cR_\lambda^{3/2}/15^{3/4} \; , \quad c = A/a \qquad (26)$$

for some dimensionless coefficient, c, which should be of the oder of, though somewhat less than, unity. Thus, if c is specified, then Eq. (26) fixes γ and Eq. (25) determines ℓ. In comparing the data with Eq. (19) $\rightarrow$ (21), therefore, we need only settle on the value of c.

Now A, and hence c, is non-universal and may vary from one geometry to another. Indeed energy decay measurements for the two grids show that the ratio of A is $A_{con}/A_{mod} = 1.33$, and so we require c for the conventional mesh to be 33% higher than that for the modified grid. For the present purposes, we have chosen $c = 0.337$ for the modified grid and $c = 0.448$ for the conventional mesh.

Figures 9a) to 9d) show the comparison of Eq. (19) $\rightarrow$ (21) with the measured structure functions for the modified grid (R_λ = 290, 440, 550 and 660), while figures 10a) and 10b) show the comparison for the conventional grid (R_λ = 250 and 320). The comparison is striking for both sets of data, confirming the mixed power-law behaviour of $\langle(\Delta v)^2\rangle$ in the inertial range. In order to emphasise the point, Figure 9 and 10 also show the pure power-law estimate of $\langle(\Delta v)^2\rangle$, Eq. (22), based on the traditional interpretation of $\langle(\Delta v)^2\rangle$ in which the enstrophy contribution is neglected, i.e.

$$\frac{3}{4}\langle(\Delta v)^2\rangle = \int_{\pi/r}^{\infty} E(k)dk \; . \qquad (27)$$

The fit is much less satisfactory, as we would expect.

a) $R_\lambda = 290$

b) $R_\lambda = 440$

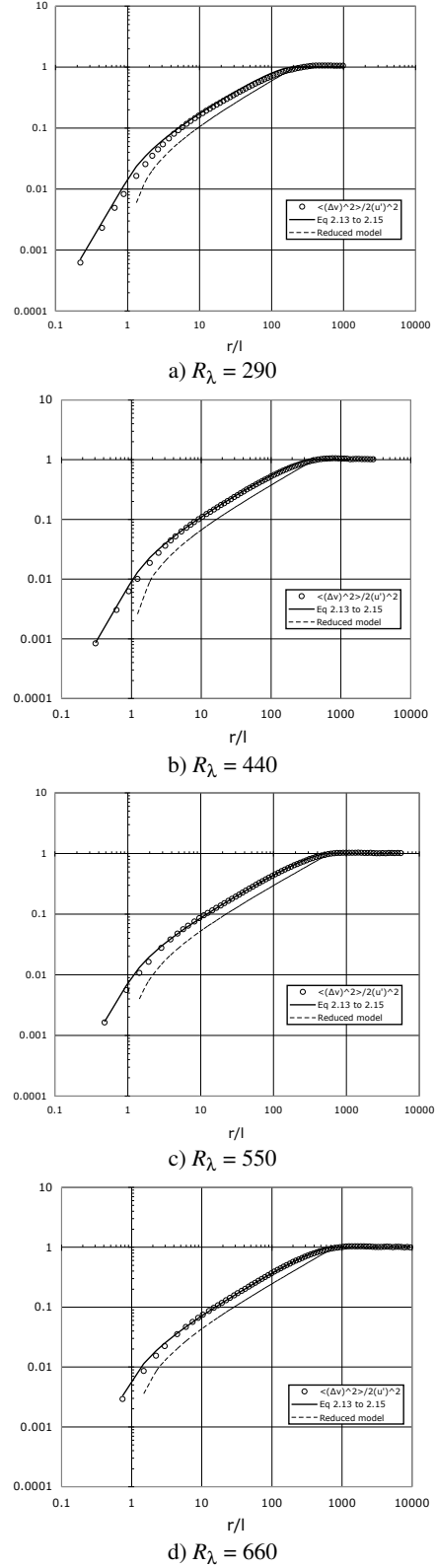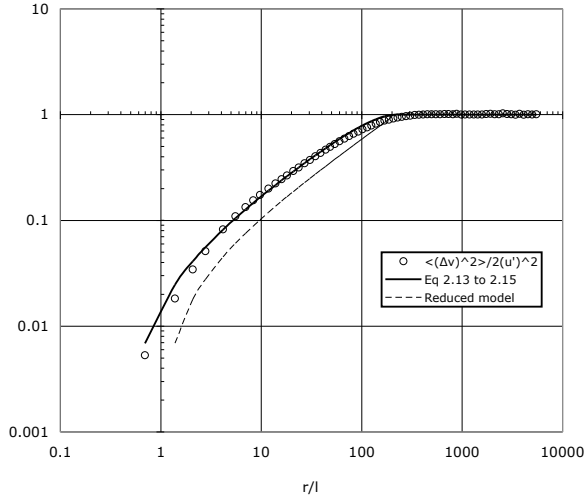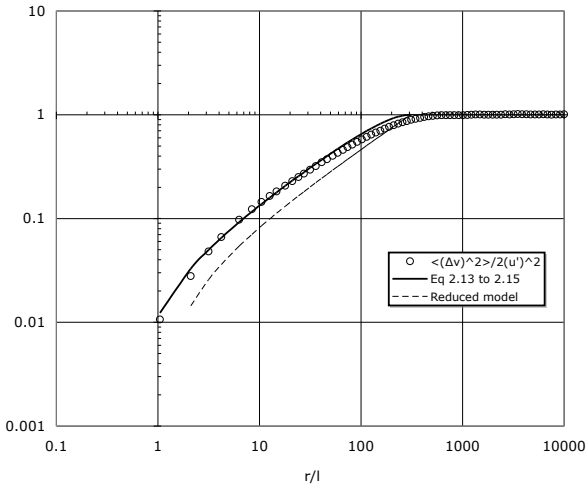c) $R_\lambda = 550$

d) $R_\lambda = 660$

Figure 9: Comparison between the measured $\langle(\Delta v)^2\rangle$ /2 and equations (19)-(21) for the modified grid. Symbols are measurements and curves the theoretical predictions. The dashed line represents the pure power-law, equation (22).

549

a) $R_\lambda = 250$

b) $R_\lambda = 320$

Figure 10: Comparison between $\langle (\Delta v)^2 \rangle /2$ and equations (19)-(21) for the conventional grid. Symbols are measurements. The dashed line represents the pure power-law, equation (22).

Note that, for large γ, Eq. (22) simplify to

$$\frac{(3/4)\langle (\Delta v)^2 \rangle}{<\mathbf{u}^2>/2} = (r/L)^{2/3} \quad , \quad \ell << r < L \qquad (28)$$

which is independent of γ, and hence of c and R_λ. Thus the main differences between the combined power-law form of $\langle (\Delta v)^2 \rangle$, which is an excellent fit to the data, and the spurious single power-law estimate of $\langle (\Delta v)^2 \rangle$, which comes from Eq. (27), are independent of the choice of the coefficient c. The single power-law estimate of $\langle (\Delta v)^2 \rangle$ is clearly inferior.

Conclusions

We have shown that the second-order structure function is a poor filter, in the sense that it mixes information from large and small scales and information about energy and enstrophy. One consequence of this is that, in the inertial range, it takes the form of a mixed power-law of the form, $\langle (\Delta v)^2 \rangle \sim a_1 + a_2 r^2 + a_3 r^{2/3}$ with r^2 tracking the enstrophy of the eddies and $r^{2/3}$ tracking the energy. This is the reason why Kolmogorov's two-thirds law is harder to realise than the equivalent spectral 5/3's law. We have illustrated this with a simple model problem which gives a surprisingly good fit to measurements made in grid turbulence.

We emphasise that it is not just the second-order structure function which suffers from this problem, all even-order structure functions mix information from large and small scales, and this calls into question the physical interpretation of measured anomalous scaling exponents for higher-order structure functions.

References

[1] Davidson, P.A., *Turbulence, An introduction for Scientists and Engineers*, Oxford University Press, 2004.

[2] Davidson, P.A. & Krogstad, P.-Å., On the Deficiency of Even-Order Structure Functions as Inertial Range Diagnostics. Submitted to *J. Fluid Mech.*, 2007

[3] Landau, L.D. & Lifshitz, L.M., *Fluid Mechanics. 2nd ed.* Pergamon Press, 1986.

[4] Monin, A.S. and Yaglom, A.M., *Statistical Fluid Mechanics II*, MIT Press, 1975.

[5] Townsend, A.A., *The Structure of Turbulent Shear Flows.* 2nd edition, Cambridge University Press, 1976.